

## **Directional characteristics of shallow water waves along southwestern Bay of Bengal**

Johnson Glejin, V. Sanil Kumar\*, T.R.Anoop, Jofia Joseph

Ocean Engineering Division, CSIR-National Institute of Oceanography (Council of Scientific & Industrial Research), Dona Paula, Goa 403 004 India URL, [www.nio.org](http://www.nio.org)

\*Correspondence to: Tel.: 0091 832 2450 327 Fax: 0091 832 2450 602 email: [sanil@nio.org](mailto:sanil@nio.org)

### **Abstract**

The aim of the present research is to investigate the directional characteristics of waves along the southwestern Bay of Bengal based on the measured data during 2010 at 14 m water depth. Diurnal, monthly and annual variation of reflected waves is studied for waves within a frequency range of 0.03 - 0.125 Hz to eliminate the influence of local wave growth processes. High values of directional width during the annual cycle over the southwestern Bay of Bengal is associated with the swell reflection from the coast during southwest monsoon season (June-September) and intrusion of moderate easterly winds propagating from Gulf of Thailand over the narrow land mass of Thailand and Myanmar. The reflected wave energy is maximum (14%) during the southwest monsoon due to the presence of long period and intermediate period waves and minimum (9%) during the northeast monsoon season (October-January). During fair-weather period (February-May), 10% of the total energy is propagated towards offshore. We also analyzed the relationship between directional and non-directional wave parameters using continuous wavelet transform and wavelet coherence analysis (WCA). WCA shown that reflection coefficient and total energy is directly/inversely proportional to the swells, when signal of period approximately less/greater than one day is observed.

**Key Words:** Ocean sciences, surface waves, directional wave spectrum, reflected waves

## 1. Introduction

The wave directional characteristics of the sea states is a vital input variable in the design of marine structures, wave forecasting, shore protection and design of vehicles. Availability of measured data on wave directional spreading are limited and the designers have only estimates of wave height, period, direction, and theoretical models of wave directional spectra are used to generate representative wave conditions for practical applications (Lee et al., 2010). Directional spectrum is generally represented as a product of the frequency spectrum and the directional spreading function (Borgman, 1982) and the directional spreading function is estimated using parametric models (Longuet-Higgins et al., 1963; Borgman, 1982; Donelan et al., 1985). In most parametric models, mean wave direction ( $\theta$ ) is an input parameter (Kuik et al., 1988). The parameter used to estimate the directional spreading function is the spreading parameter ( $s$ ). The studies on the directional spreading of shallow water waves are limited (Ewans, 1998; Herbers et al., 1999; Sanil Kumar et al., 1999, Sanil Kumar et al., 2000; Deo et al., 2002; Sanil Kumar, 2006; Lee et al., 2010; Sanil Kumar and Anoop, 2013).

Wave reflection from natural beaches and coastal structures influence the hydrodynamics and sediment dynamics in the nearshore area. Energy and direction associated with reflected wave will also influence the directional properties of the nearshore waves (Ardhuin and Roland, 2012). Wave reflection at the shoreline is added as an important parameter in the recently developed third generation wave model WAVEWATCH III (Ardhuin and Roland, 2012), whereas Benoit et al. (1996) and Booij et al. (1999) provide an option for reflection in wave modeling. Elgar et al. (1994) found that, on natural beaches reflection is generally weak and is less than 5% of the wind-sea and swell wave energy. Studies dedicated to wave reflection are limited and only a preliminary study is carried out by Anoop et al. (2014) on the reflected/offshore propagating waves along the Indian subcontinent. Studies related to free surface gravity wave simulation in the Bay of Bengal (BoB) still uses only the growth, refraction and decay components to solve wave balance equation (Aboobacker et al., 2009). Seasonal changes in winds of east coast of India with winds from southwest (SW) during the SW monsoon period (June to September) and from northeast (NE) during the NE monsoon period (October to January) produce similar changes in the directional wave parameters and the nature of this seasonal variability is not studied. Glejin et al. (2013) studied the monsoon and cyclone induced wave characteristics over the southwestern BoB.

Wavelet transform is a recently developed analysis technique which expand time series into time frequency space and can find localised intermittent periodicities (Grinsted et al., 2004). By

decomposing a time series into a time-frequency space, the dominant modes of variability and the variation of those modes with time can be determined (Erol, 2011). Erol (2011) applied the wavelet analysis (continuous wavelet transform, cross wavelet transform and wavelet coherence algorithms as extensions of wavelet analysis) to sea-level observations recorded by tide-gauge sensors. The continuous wavelet transform (CWT) expands a time series into a time frequency space where oscillations can be seen in a highly intuitive way. Erol (2011) observed that in the time-frequency analysis of the series and inspection of the coherence between two time series, the wavelet tool CWT is very useful and practical. The wavelet transform of the length of day, atmospheric angular momentum and the southern Oscillation Index during January 1970 to June 1999, indicate that they have similar time-varying spectral structure (Zhou et al., 2001). Elsayed (2006) applied the wavelet bicoherence to study the wind-wave interaction. Wavelet coherence analysis (WCA) is a powerful method for testing proposed linkages between two time series. Wavelet bicoherence is used for analyzing wind-wave interaction (Elsayed, 2006). Camayo and Campos (2006) applied wavelet transform in the study of coastal trapped waves off the west coast of South America.

Hence in this article, directional characteristics of waves during one year period at a location in the southwestern BoB (at 14 m water depth) are studied based on the measurements carried out using a moored buoy. In addition, directional spreading of wind-sea and swell are studied. The objective of the research is to investigate the directional characteristics of shallow water waves in the southwestern BoB. Following research questions are addressed, What is the seasonal variation of directional width? How the directional spectrum changes with swells from the South Indian Ocean? What is the percentage of reflected energy along the east coast and its influence on directional characteristics ?

## **2. Materials and methods**

Measured wave data off Puducherry, southwestern BoB (Figure 1) during 1 January to 31 December 2010 using the directional wave rider buoy, DWR Mk-III at 14 m water depth ( $11^{\circ} 55' 26''$  N latitude and  $79^{\circ} 51' 03''$  E longitude) are used for the study. The wave rider buoy measures free surface gravity waves with heaves in the range of -20 and +20 m, with a resolution of 1cm in heave, and periods between 1.6 and 30 s. The cross sensitivity of the heave is less than 3%. The range of measurement of the wave direction using DWR Mk-III is  $0-360^{\circ}$  with a resolution of  $1.5^{\circ}$  and an accuracy of  $0.5^{\circ}$  and is reference to the magnetic north. Data are recorded continuously at 1.28 Hz, and the data for every 30 min are processed as one record. The collected time series is subjected to standard error verification for spikes, steepness and constant signals and a total of 17517 records are

used for further analysis. Measurements are made in Coordinated Universal Time (UTC) and the time referred in the paper is in UTC. The wave spectrum is obtained via the Fast Fourier transform (FFT) of the measured vertical elevations of the buoy. At the low frequency end accelerations become very small and disappear in the sensor noise. Therefore, a digital high-pass filter with a cut off at 30 s (0.033 Hz) is applied to the samples. At higher frequencies, the wave wavelength becomes comparable to the buoy dimensions and the buoy will not be able to follow the particular waves anymore (geometric attenuation) (Datawell, 2009). As higher frequency measurements can only introduce noise, all outputs of the buoy sensors are filtered by applying a low-pass filter with a cut off frequency of 0.58 Hz. The frequency resolution is 0.005 Hz for frequency 0.033 to 0.1 Hz and is 0.01 Hz for frequency higher than 0.1 Hz. Significant wave height ( $H_{m0}$ ) is obtained from the spectral moment. Period corresponding to the maximum spectral energy, i.e., spectral peak period ( $T_p$ ) is obtained from the wave spectrum. Mean wave direction ( $\theta$ ) is estimated based on Kuik et al. (1988). Directional spreading is studied using directional width ( $\sigma$ ) as given by Kuik et al. (1988) and mean spreading angle ( $\theta_k$ ) according to Goda et al. (1981). The details of wave parameters used in the study are presented in Annexure (Sanil Kumar and Anoop, 2013). Coastal inclination along the Puducherry coast is  $15^\circ$  to the north in the NE-SW inclination and hence  $15$  to  $195^\circ$  waves approach the coast. The waves with direction more than  $195^\circ$  and less than  $15^\circ$  will be propagating away from the coast. Energy associated with onshore ( $E_{in}$ ), offshore ( $E_{out}$ ), and total ( $E_{tot}$ ) propagating waves is calculated as,

$$E_{in} = \int_{0.03}^{0.58} \int_{15^\circ}^{195^\circ} E(f, \theta) d\theta df \quad (1)$$

$$E_{out} = \int_{0.03}^{0.58} \int_{195}^{360} E(f, \theta) d\theta df + \int_{0.03}^{0.58} \int_0^{15} E(f, \theta) d\theta df \quad (2)$$

$$E_{tot} = \int_{0.03}^{0.58} \int_0^{360} E(f, \theta) d\theta df \quad (3)$$

Percentage of onshore and offshore energy are calculated as the ratio between  $E_{in}$  or  $E_{out}$  to  $E_{tot}$  at the measurement location. NCEP/NCAR reanalysis data (Kalnay et al., 1996) of zonal and meridional components of wind speed at 10 m height real-time observations at 6 hour intervals is used to study the wind pattern. The meteorological convention is used for presenting the wind and wave direction data ( $0$  and  $360^\circ$  for wind/wave from North,  $90^\circ$  for East,  $180^\circ$  for South,  $270^\circ$  for

West). Wave age is estimated as  $C_p/U$ , where  $C_p$  is the wave celerity at peak frequency and  $U$  is wind speed.

We used CWT and wavelet coherence analysis (WCA) (Grinsted et al., 2004) to examine the power spectrum and coherence of incident and reflected wave parameters.

### **3. Results and discussions**

#### **3.1. Directional spreading of waves**

Directional width indicates the broadness of the directional spectrum with high (low) values for board (narrow) banded directional spectrum. Directional spreading is narrowest with low values at the spectral peak ( $f_p$ ) and broad at frequencies both higher and lower than  $f_p$  (Figure 2a) similar to the earlier observations (Mitsuyasu et al., 1975; Hasselmann et al., 1980; Sanil Kumar and Anoop, 2013). During the NE monsoon period, average value of the directional width is less ( $25^\circ$ ) than the annual average value ( $27^\circ$ ). The contour plots of normalized wave spectral energy density with frequency and time during 2010 are plotted to study the variations in wave spectral energy density and to show the presence of wind-seas and swells (Figure 2b). The normalised spectral energy density is obtained through dividing the spectral energy density at different frequency by the maximum spectral energy density of that spectrum, similar to the analysis reported in Sanil Kumar and Anjali Nair (2015). Predominance of the wind-seas are observed during February to May and in November and December (Figure 2b). During the SW monsoon period, relatively large values of directional width are observed due to the co-existence of long period swell waves and wind-seas in the study area (Glejin et al., 2013). The low values of directional width observed during the SW monsoon period are confined to a narrow frequency range (0.08-0.15 Hz) (Figure 3a). During the NE monsoon period, except in October, due to the dominance of wind-sea, the low values of the directional width are predominantly in the high frequencies (Figure 2a). When the swell is predominant, in October, the low values of directional width are shifting towards lower frequencies (Figure 2a). The low-frequency waves in the study area are mainly from  $120$  to  $150^\circ$ , whereas the direction of high-frequency waves changes with seasons. High frequency waves during January-February and November-December are from  $60$  to  $90^\circ$  and during February-May are from  $120$  to  $150^\circ$  and during June to October are from  $150$ - $180^\circ$  (Figure 2c).

$H_{m0}$  of the waves from SE is less than 1.6 m and the increase in wave height is not observed with increase in peak wave period since the waves from SE are mainly swells. A trend of increasing directional spread with decreasing wave energy is observed for these SW swells similar to the

observation of Herbers et al. (1999). The directional width for high waves ( $H_{m0} > 2$  m) is less with average value of  $19^\circ$  compared to the annual average value of  $27^\circ$  (Figure 3a). During the measurement period, two cyclonic storms, Laila (17-20 May 2010) and Jal (4-8 November 2010), influenced the waves in the southwestern BoB (Figure 1). The Tropical Cyclone Laila had maximum sustained winds of 33.3 m/s on 19 May 2010. The storm had moved towards the north-northwest over the previous several hours (Angove and Falvey, 2010). When the cyclone Laila and Jal are near the study area, a sudden drop in directional width ( $\sim 10.5^\circ$ ) is observed, whereas the directional width of more than  $20^\circ$  persisted during the pre-cyclone period. In the post-cyclone period, the directional width increased to pre-existing value ( $> 20^\circ$ ). This significant drop in directional width is caused by storm generated waves with high energy towards the coastline which are constrained to a region by fetch limited sea where the waves are generated by the cyclone winds (Forristall and Ewans, 1998; Buchan et al., 1999).

A decreasing trend in directional width is found for swell dominated waves with decrease in peak wave period (Figure 3b). After reaching the minimum directional width, an increasing trend in directional width is observed for the high frequency waves. To check whether this is only a phenomenon observed during the year 2010, we analyzed the measured wave datasets for 2009 and 2011. It is found that the transitions towards lower and higher  $T_p$  are observed in all three years (2009, 2010 and 2011) (Figures not presented). Further analysis on direction together with the former parameters indicate that, the increase in directional width towards lower  $T_p$  arise from the waves propagating from the NE and E direction. These waves are associated with broad directional distribution in the wind-sea/short period waves ( $T_p < 8$  s) part of the spectrum. These types of waves with low peak period and large directional width are observed mainly during the fair-weather (FW) period (Feb-May) and NE monsoon period and are negligible during the SW monsoon period due to the strong SW winds.

Directional spread is one of the important factors which influence the nonlinear characteristics such as wave skewness, wave asymmetries (Prevosto, 1998) and radiation stress (Feddersen, 2004). So it is important to identify why these factors such as lower peak period and directional width are concomitant only during the FW and NE monsoon season and not in the SW monsoon season at the southwestern BoB. Wind-sea is generated by the local wind system and here, we are interested in the short period waves reaching the study location. For this we analyzed the wind pattern over the entire BoB during which we observed easterlies with moderate strength blows from the Andaman Sea during the NE monsoon season and this may be the reason for higher directional width observed off Puducherry. To find out more clarity about this easterly wind we further extended the region towards

the western pacific. It is found that NE winds blowing through the South China Sea reaches the Gulf of Thailand and changes its direction as easterlies and crosses the narrow land mass over the Thailand and Myanmar which separating Gulf of Thailand and Andaman Sea and to the BoB. This propagation of easterlies from the Gulf of Thailand is observed during the starting of FW and NE monsoon season when NE winds blows over the BoB region (Figure 4). During the strong SW monsoon season, the SW winds blocks the NE winds from the South China Sea and enters into the Gulf of Thailand as easterlies and turned the N-Easterlies to S-Westerlies. This unidirectional SW wind and coastal plain over the west side of the wind diminishes the wind-sea generation by these seasonal winds. During this season wind-sea is generated by the local wind climate as sea/land breeze and swells observed at the coast is by the remotely generated waves in the southern Indian Ocean (Glejin et al., 2013).

In the FW and NE monsoon season, wind climate over the northern BoB mainly depends on the north-easterly winds, whereas the nearshore region of study location situated at the southern part of India is influenced by two wind systems, 1) NE monsoon winds and 2) E-SE winds propagating towards the southeastern part of Indian coast during the FW and NE monsoon season. The presence of these two wind systems over the central BoB, off Puducherry causes the wind-sea generation from large area and increases the directional spread associated with short period waves reaching the study location.

The estimated value of peak wave period is  $\sim 6$  s at which the transition towards higher ranges in directional width occurs. Maximum directional width persisted for waves propagating towards the nearshore regions of the study area with maximum peak wave period. On an average, the directional spreading of the swell dominated spectrum is higher (directional width  $\sim 26^\circ$ ) than that of wind-sea dominated wave spectrum (directional width  $\sim 23^\circ$ ). In deep waters, the directional spread at the peak frequency is about  $10^\circ$  for swells and  $30^\circ$  for wind-seas (Forristall and Ewans, 1998). Since the measured data consists of wind-seas and swells, large difference in values of directional width is not observed. Even though the SE waves are the narrow banded swells with low wave height, due to the co-existence of wind-sea, high value of directional spread are observed for the SE waves (Figure 3c).

The variation of directional width with wave age values is similar to the observation of Banner and Young (1994). The directional spread increases slightly as the wave age decreases (Figure 3d). The directional width is low for highly positively skewed surface elevation since the high sea states are positively skewed (Figure 3e). The values of  $\sigma$  are larger than those of  $\theta_k$  (Figure 3f) similar to the

earlier observations (Goda et al., 1981; Benoit, 1992 and Besnard and Benoit, 1994; Sanil Kumar, 2006). Average value of  $\sigma$  is  $27^\circ$  and the corresponding value of  $\theta_k$  is  $17^\circ$ .

### 3.2. Directional spectrum

Based on numerical test cases, Hashimoto et al. (1993) observed that for single point measuring system, Extended Maximum Entropy Method (EMEM) estimates better directional spectrum. Since the data used in the study are from a wave rider buoy (single point measuring system), EMEM is used for the estimation of directional spectrum. From the half hourly data, the monthly averaged directional spectrum is estimated to study the directional wave properties (Figure 5). Monthly averaged directional spectrum shows the energy distribution of waves propagating into the nearshore regions. A low energy peak from the western side, which is restricted by the coastal land is observed in the monthly averaged directional wave energy spectrum due to the waves reflected from the coastline (Figure 5). The reflected waves show a variation in energy and are a minimum during the wind-sea dominated NE monsoon and at the start of the calm FW period. This indicates that during the swell dominated period, high values of directional width is also associated with the waves reflected from the coast together with the incident swells (Ardhuin and Roland, 2012).

Maximum spectral energy for wind-sea is observed in the month of December and January (NE monsoon season) due to the NE monsoon winds because of its restricted fetch due to land boundaries in the northern part of BoB. The spectral energy of incident waves is also from the NE ( $65-90^\circ$ ) (Figure 5). Corresponding maxima for the swells is observed during September in the SW monsoon season due to the propagation of south-easterly swells from the south Indian Ocean and Southern Ocean (Glejin et al., 2013). NE monsoon season is dominated by the high frequency (0.15-0.25 Hz) waves (Figure 6b) and at the end of the NE monsoon season, from March onwards the spectral energy is shifting towards very high frequency region (0.25-0.4 Hz) due to the weakening of NE monsoonal winds which results in the setting up of local sea/land breeze system. During the FW period, smaller wave heights ( $H_{m0} < 0.75$  m) are observed due to the limited fetch and seaward wind direction (Figures 6a and 2d).

In the later stages of SW monsoon, wave energy concentrates towards the low frequency region due to the increase in swells from the SE because of westerly winds in the south Indian Ocean and frequent storms in the Southern Ocean and weakening of high frequency wave generating sea/land breeze system. When the NE monsoon starts, wave energy propagates back towards the high frequency region and has two peaks during December due to SE swells and NE wind-sea. This trend



continues to persist and accumulates with an energy peak at the high frequency region during January and February.

### **3.3. Onshore-offshore /reflected waves**

Onshore-offshore wave propagation is another factor influencing the wave directional characteristics. In this section, the onshore-offshore/reflected wave characteristics are described (Table 1). Puducherry coastal contours make an angle of  $15^\circ$  to the north in the NE-SW inclination. The bottom contours and refraction change the swells towards the normal at the study location with incident angle of  $105^\circ$ . When the swells incident on the shoreline, it reflects some of its energy directly back towards the offshore direction and this propagates towards ocean as reflected waves. Along the east coast of India, the propagation of swells are dominated from the SE direction, whereas the NE swells are limited and only observed during the high windy conditions such as storms and cyclones over the northern BoB. This makes the swells reaching the SE direction ( $\sim 120^\circ$ ) and incident at the shore at an angle approximately equal or slightly greater than the shore normal  $105^\circ$ . This causes the wave energy moves towards the offshore (reflected wave) from an angle of  $\sim 300^\circ$  as shown in the Figure 5.

Monthly variation of total energy and corresponding percentage of offshore propagating waves show a reverse relationship between these two parameters (Table 1). Maximum percentage of offshore wave propagation is observed during the SW monsoon season (August, 14.54 %) and minimum during NE monsoon season (January, 5.54 %). The variation of offshore propagating waves shows that it depends on the percentage of swells observed at the study region. Since the local wave growth is not an issue in the present study, the offshore propagating waves are the reflected waves and also these waves have peak energy at the swell waves with period mostly more than 8 s. Maximum energy density propagated towards offshore is in May ( $7.28 \text{ m}^2/\text{Hz}$ ) and is due to the presence of swells generated by severe cyclonic storm Laila. NE monsoon season (OND) is prone to cyclones and depressions over BoB. In 2010, BoB is characterized by three cyclones (Laila in May, Giri in October and Jal in November) and two depressions during October and one depression during December (IMD, 2011). Generation and propagation of swells towards the coast during the cyclone period causes the high energy towards offshore during October, November and December compared to January during the NE monsoon period. The seasonal winds observed at the specified location are either NE or SW in the BoB area. Hence, the wind will not play a role in the growth of swell waves from the NW direction even if the measurement location is not close to the shore.

### 3.4. Influence of wind-sea on reflected waves

Wind climate over the western BoB is characterized by sea-land breeze system with maxima during the SW monsoon period and feeble during the NE monsoon season. Having this nearshore wind pattern, the wave climate over the study region is dominated by wind-sea over swells during most of the time (Glejin et al., 2013). Hence, it is important to analyse the effect of wind-sea on the reflected waves over the region to know what are the parameters influencing the reflected waves besides the bathymetry and tidal effects (Anoop et al., 2014; Ardhuin and Roland, 2012; Nelson and Gonсалves, 1990) in the nearshore region. For this we analyzed the diurnal variation of reflected wave and wind-sea energy over the annual cycle by averaging the wave properties in each hour (Figure 7).

Earlier study by Glejin et al. (2013) shown that the study area is under the influence of sea-breeze generated wind-sea in a diurnal pattern with minimum during the early morning hours and maximum during the late evening hours. In the present study also we observed similar pattern of  $H_{m0}$  over the nearshore region (Figure 7). To study the swells and its role in the region, we separated the total swell energy into two parts, as incident and reflected swell part (Elgar et al., 1994) and analyzed here.

Monthly average of hourly variation over daily cycle of reflected waves show a semi-diurnal pattern in reflected wave energy with slightly different peak value. This semi-diurnal pattern is not much evident in the incident swell energy, mainly during the NE monsoon when strong NE wind is blown over the region. The first peak of the hourly variation is concurrent with a peak in incident swell energy and trough in total  $H_{m0}$  (wind-sea and swell). However, the second peak in the reflected energy is observed with the peak in  $H_{m0}$  irrespective of the incident swell energy. The study shows that the short period waves play a role in the energy of reflected wave in the nearshore region since the daily variation in total wave height ( $H_{m0}$ ) over the nearshore region mainly depends on the wind-sea height over the region, whereas the swell height is observed as constant throughout the day (Glejin et al., 2013). Another observation of the study is the increase in energy of reflected swells propagating towards offshore direction coincides with the oppositely propagated wind-sea generated sea breeze. This observation contradicts the maser mechanism proposed by Longuet and Higgins (1969), which suggests damping of long waves if long waves and short waves are propagating in opposite directions, as for wind blowing against a swell. Garrett and Smith (1976) shown that long waves can grow if short wave generation (rather than dissipation) is correlated with the long wave orbital velocity. Another study by Ardhuin and Jenkins (2006) indicates that long waves growth rate is the sum of growth rates by the sum of wind-sea modulation, roughness and orbital velocity

modulation in the wind input, direct momentum into waves and energy absorbed from the turbulent flux.

### **3.5. Wavelet analysis**

CWT applied to the time series data on  $H_{m0}$ , reflected swell coefficient, directional width and skewness to know the temporal variability. WCA applied to two time series to identify the region of strong local correlation between the two time series and also to know the phase relationship. The time series pairs used in the WCA are i)  $H_{m0}$  and reflected swell coefficient, ii)  $H_{m0}$  and directional width, iii) reflected swell energy and skewness, iv) reflected swell energy and kurtosis, v) directional width and reflected swell coefficient, vi) directional width and maximum spectral energy density, vii) directional width and peak period and viii) directional width and skewness. The coherency scale shown is between zero (Blue) to one (Red). Red regions in the plots indicate frequencies and times for which the two series share variability.

#### **Continuous wavelet transform**

Morlet power wavelet spectrum of  $H_{m0}$  (Figure 8a) clearly shows that energy peak in the one day period is dominant during the FW and SW monsoon, whereas the high energy during November with 2-8 day band is due to the cyclonic storm Jal which passes near the measurement location. Further we analysed the reflection of swell from the coast using CWT (Figure 8b) to identify the temporal variability of energy. A band of significant peak over the 0.5 day oscillation, corresponds to the semi-diurnal tidal influence, with lesser energy peak at 1 day period are observed. The peak in reflected energy at 0.5 day oscillation is mainly concentrated during the months of SW monsoon season, due to the swell domination off the east coast of India (Glejin et al., 2013). The main difference between the features in the wavelet power in  $H_{m0}$  and reflected swell is the maximum energy observed at the diurnal and semi-diurnal scales.  $H_{m0}$  spectra show maximum energy during the 1 day period, whereas reflected swell is at 0.5 day oscillations. Both series also have high power in the 4-64 days band. Directional width shows 0.5 day oscillation during July to October along with oscillations with higher period (Figure 8c). Morlet power wavelet spectrum of skewness is similar to that of  $H_{m0}$  (Figure 8d).

#### **Wavelet coherence analysis**

Coherence spectrum between  $H_{m0}$  and reflected waves (Figure 9a) in the swell band (8-30 s) shows that at 1 day oscillation both time series are in phase for first half of the study period and covariance is mainly restricted to 1 day period where influence of sea-land breeze effect and NE monsoon

induced wind-sea generation are dominant in the annual cycle. While during the second half of the annual cycle covariance is observed during the higher period oscillations (8-32 days). During this time period, the measurement location is characterised by waves in the intermediate and long period waves (Glejin et al., 2013). The influence of wind-sea on reflected swell is negligible compared to the first half in the annual cycle. The in-phase relationship between  $H_{m0}$  and swell reflection during the NE monsoon and FW and out of phase between during the swell dominated SW monsoon season indicates the role of wind-sea factor in the direct and indirect co-variation between  $H_{m0}$  and swell reflection energy in an annual cycle. Coherence spectrum between  $H_{m0}$  and directional width (Figure 9b) shows that both time series are out of phase during the annual cycle, but shows oscillations with higher period (8-32 days).

To understand the influence of kurtosis on swell reflection coefficient we have carried out the wavelet coherence analysis, but we could not find any strong relationship between these two variable. The coherence spectrum (Figure 9d) clearly indicates that strong coherence is only observed as patches of energy within periods of 2-32 days oscillations and both variables are appeared in out of phase during the period. Two most dominant coherence observed in the spectra in May and November are during the cyclones Laila and Jal.

Ardhuin and Roland (2012) studied the concomitant behaviour of directional spread with wave reflection at the shoreline and found that directional spread depends on the wave reflection using WAVEWATCH III model. We studied the mutual dependence of these two wave properties using the wavelet approach. WCA of directional width and reflection coefficient (Figure 10a) shows that maximum coherence is observed with 0.5 and 1 day periods in the high frequency region and another in the 8-24 days oscillation during the months of August to December. It is also observed that both variables are in phase during the dependency periods. Half day and one day oscillations are due to the influence of semi-diurnal mixed tides observed in the reflection coefficient (Anoop et al., 2014). Anoop et al. (2014) observed that, wave trapping and energy dissipation due to bottom friction during the low tides cause variation in reflection coefficient along the Indian coastal waters. Low frequency band at 8-24 days oscillations are due to the presence of swells generated by frequent cyclonic storms in the BoB and also in the western Australian region within the south Indian Ocean. Coherence spectrum between directional width and  $T_p$  shows that both time series are in phase during the annual cycle (Figure 10c), but directional width and maximum spectral energy density are out of phase (Figure 10b).

The present study shows that directional width is directly related to the swell wave reflection at the shoreline and is similar to the observation of Arduin and Roland et al. (2012). We also observed a direct relationship between skewness and swell reflection (Figure 9c), but the WCA spectrum between skewness and directional width (Figure 10d) shows both parameters are in out of phase when coherence is observed. The skewness decreases when the directional spreading increases (Prevosto, 1998) because as the  $T_p$  increases swells are more prone to shoal due to bathymetry and then they become skewed (Gonzalez-Rodriguez, 2007) without a decrease in directional width.

#### **4. Conclusion**

We studied the directional characteristics of shallow water waves off Puduchery, located along the southeastern BoB, based on the wave data measured during 2010 at 14 m water depth and with the help of continuous wavelet transform (CWT) and wavelet coherence analysis (WCA). Observations reported here on directional width support the previous findings in the nearshore region. Relatively high values of directional width are observed during the SW monsoon (June-September) due to the co-existence of long period swell waves and wind-seas in the study area, whereas during the wind-sea dominated FW (February-May) and NE monsoon period (October-January) the low values of directional width are shifted towards lower frequency part of the spectrum. During the cyclones, a sudden reduction in directional width from  $20$  to  $10.5^\circ$  is observed. A contradictory trend found in the peak wave period-directional width diagram from the previous studies shown an increase in directional width towards higher frequencies (lower periods) due to the propagation of short period waves to the measurement site generated by easterly winds, the wind blowing over the narrow land mass of Thailand and Myanmar, as the extension of the Pacific trade winds. The estimated value of peak wave period is  $\sim 6$  s at which the transition towards higher ranges in directional width occurs.

Another factor influencing the directional spread is the wave reflection. Monthly average directional spectrum shows that during the SW monsoon, wave energy concentrates towards the low frequency region due to the increase in swells from the south Indian Ocean. Average percentage of offshore propagating wave energy is 14% in SW monsoon, 9% in NE monsoon and 10% during FW period. The spectral energy of reflected waves is maximum during the swell dominated period. One of the significant findings of the study is the dependence of reflected swell energy with the short period waves in diurnal cycles. Growth in reflected wave energy during the wind-sea domination is due to either by short wave generation and long wave orbital velocity or by momentum transfer from roughness or turbulent flux.

The wavelet power spectra of  $H_{m0}$  and reflected swell clearly indicate the diurnal (sea/land breeze) and semidiurnal (tidal) oscillation in the observations. Similar pattern (diurnal and semidiurnal) is also observed in the skewness and directional width spectra. Coherence spectrum between  $H_{m0}$  and reflected waves in the swell band (8-30 s) shows that oscillation of period less than 2 days are in-phase during which wind-sea generated sea-land breeze dominates, whereas during the swell dominant period these variables are independent (out of phase) to each other. Wave reflection shows coherence to kurtosis only when strong a turbulent condition such as cyclonic storms prevails.

### **Acknowledgments**

The authors gratefully acknowledge the financial support given by the Earth System Science Organization, Ministry of Earth Sciences, Government of India to conduct part of the research. The Director of the CSIR-National Institute of Oceanography, Goa and the Director of the INCOIS, Hyderabad provided encouragement in carrying out the study. We thank Dr. T.M. Balakrishnan Nair, Head OSISG, Mr. Arun Nherakkol, Scientist, Mr. C. Jeyakumar, INCOIS, Hyderabad and Mr. Jai Singh, Technical Assistant at CSIR-NIO for assistance during the data collection. We thank Pondicherry Multipurpose Social Service Society, Puducherry for help provided during the measurement. The wind data used in the study are provided by the NOAA-CIRES Climate Diagnostics Center, Boulder, Colorado at <http://www.cdc.noaa.gov/>. Wind data obtained from [http://apps.ecmwf.int/datasets/data/interim\\_full\\_daily/](http://apps.ecmwf.int/datasets/data/interim_full_daily/) are used to show the monthly wind pattern in Figure 4. We thank the reviewers for the critical comments and the suggestions that improved the paper. This work is NIO contribution No. xxxx.

### **Annexure: Definition of wave parameters used in the study**

$$\text{Significant wave height } (H_{m0}) = 4\sqrt{m_0} \quad (A1)$$

$$\text{Mean wave period } (T_{m02}) = \sqrt{m_0/m_2} \quad (A2)$$

Where  $m_n$  is the nth order spectral moment given by,  $m_n = \int_0^\infty f^n S(f) df$ ,  $n=0$ , and 2

$S(f)$  is the spectral energy density at frequency  $f$ .

Mean wave direction ( $\theta$ ) is estimated as below (Kuik et al., 1988).

$$\theta(f) = \arctan [b_1(f)/a_1(f)] \quad (A3)$$

Where  $a_1$  and  $b_1$  are the first four Fourier coefficients of the directional distribution function and are determined as follows:

$$a_1(f) = \frac{Q_{zx}(f)}{k(f).C_{zz}(f)} \quad (A4)$$

$$b_1(f) = \frac{Q_{zy}(f)}{k(f).C_{zz}(f)} \quad (A5)$$

where,  $C_{xx}$ ,  $C_{yy}$  and  $C_{zz}$  represents the auto spectra,  $C_{zx}$  the co-spectra and  $Q_{zx}$  the quadrature spectra between variables  $z$  and  $x$ ,  $C_{xy}$  the co-spectra between variables  $x$  and  $y$ ,  $Q_{zy}$  the quadrature spectra between variables  $z$  and  $y$ ,  $k = \sqrt{\frac{C_{xx}(f) + C_{yy}(f)}{C_{zz}(f)}}$  is the wave number determined from the auto spectra.

Variables  $z$ ,  $x$  and  $y$  represents the 3-translational (vertical, north-south and east-west) motions of the directional waverider buoy.

Directional width ( $\sigma$ ) as given by Kuik et al. (1988) and mean spreading angle ( $\theta_k$ ) as per Goda et al. (1981) are used to study the directional spreading.

$$\sigma = \sqrt{2(1-r_1)} \quad (A6)$$

$$\theta_k = \arctan \left[ \frac{\sqrt{0.5 b_1^2 (1 + a_2) - a_1 b_1 b_2 + 0.5 a_1^2 (1 - a_2)}}{a_1^2 + b_1^2} \right] \quad (A7)$$

Where,  $r_1 = \sqrt{(a_1^2 + b_1^2)}$

## References

- Aboobacker, V., Vethamony, P., Sudheesh, K., Rupali, S., 2009. Spectral characteristics of the nearshore waves off Paradip, India during monsoon and extreme events, *Nat. Hazards* 49(2), 311-323. doi:10.1007/s11069-008-9293-8.
- Angove, D. M., Falvey, J. R., 2010. Annual Tropical Cyclone Report. U.S. Naval maritime Forecast Center/ Joint Typhoon Warning Center Pearl Harbor, Hawaii. pp. 1-109.
- Anoop, T. R., Sanil Kumar, V., Glejin, J., 2014. A study on reflection pattern of swells from the shoreline of peninsular India, *Nat. Hazards* 74, 1863-1879. doi:10.1007/s11069-014-1282-5.
- Ardhuin, F., Jenkins, A. D., 2006. On the interaction of surface waves and upper ocean turbulence, *J. Phys. Oceanogr.* 36(3), 551-557. doi: <http://dx.doi.org/10.1175/JPO2862.1>
- Ardhuin, F., Roland, A., 2012. Coastal wave reflection, directional spread, and seismoacoustic noise sources, *J. Geophys. Res.(Oceans)*, 117(C11), 1-16. doi: 10.1029/2011JC007832.
- Banner, M., Young, I., 1994. Modeling spectral dissipation in the evolution of wind waves. Part I, Assessment of existing model performance, *J. Phys. Oceanogr.* 24 (7), 1550-1571.
- Benoit, M., 1992. Practical comparative performance survey of methods used for estimating directional wave spectra from heavepitch roll data, in: *Proceedings of 23rd International Conference on Coastal Engineering American Society of Civil Engineers, Venice, Italy, Vol. 2, 62–75.*
- Benoit, M., Marcos, F., Becq, F., 1996. Development of a third generation shallow-water wave model with unstructured spatial meshing, *Proceedings of 25th conference on Coastal Engineering, Orlando, Florida, 1-25.* doi:<http://dx.doi.org/10.9753/icce.v25.%25p>.
- Besnard, J. C., Benoit, M., 1994. Representative directional wave parameters-Review and comparison on numerical simulation, *International symposium, Waves Physical and numerical modelling IAHR, Vancouver, Canada, 901–910.*
- Booij, N., Ris, R., Holthuijsen, L. H., 1999. A third generation wave model for coastal regions, 1. Model description and validation, *J. Geophys. Res., Oceans* 104 (C4), 7649-7666. doi:10.1029/98JC02622.
- Borgman, L. E., 1982. Maximum entropy and data-adaptive procedures in the investigation of ocean waves, In: *Maximum entropy and bayesian methods in applied statistics*, Edited by Smith, C.R and Grandy, W.T., Laramie, Springer Netherlands, 429-442. doi:10.1007/978-94-017-2221-6\_21.
- Buchan, S., Black, P., Cohen R., 1999. Impact of tropical cyclone Olivia on Australia's northwest shelf, OTC 10791, *Proc. Offshore Technol. Conf. Houston, Texas, USA, 1-10.*
- Camayo, R., Campos, E., 2006. Application of wavelet transform in the study of coastal trapped waves off the west coast of South America. *Geophys. Res. Lett.*, 33, L22601, doi:10.1029/2006GL026395.
- Datawell, 2009. *Datawell Waverider Reference Manual*. Datawell BV oceanographic instruments, The Netherlands, pp.123.



- Deo, M.C., Gondane, D., Sanil Kumar, V., 2002. Analysis of wave directional spreading using neural networks, *J. Waterw. Port. C.-ASCE* 128(1), 30-37. doi: 10.1061/(ASCE)0733-950X(2002)128,1(30).
- Donelan, M. A., Hamilton, J., Hui, W. H., 1985. Directional spectra of wind-generated waves, *Philosophical Transactions of the Royal Society of London. Series A, Mathematical and Physical Sciences*, 315(1534), 509-562. doi:10.1098/rsta.1985.0054.
- Elgar, S., Herbers, T., Guza, R., 1994. Reflection of ocean surface gravity waves from a natural beach, *J. Phys. Oceanogr.* 24(7), 1503-1511.
- Elsayed, M.A.K., 2006. Wavelet bicoherence analysis of wind-wave interaction, *Ocean Eng.*, 33, 458-470. doi:10.1016/j.oceaneng.2005.04.013.
- Erol, S.. 2011. Time-frequency analyses of tide-gauge sensor data. *Sensors* 11, 3939–3961.
- Ewans, K. C., 1998. Observations of the directional spectrum of fetch-limited waves, *J. Phys. Oceanogr.* 28(3), 495-512.
- Feddersen, F., 2004. Effect of wave directional spread on the radiation stress, comparing theory and observations, *Coast. Eng.* 51(5), 473-481. doi, 10.1016/j.coastaleng.2004.05.008
- Forristall, G. Z., Ewans, K. C., 1998. Worldwide measurements of directional wave spreading, *J. Atmos. Ocean Tech.* 15(2), 440-469.
- Garrett, C., Smith J., 1976. On the interaction between long and short surface waves, *J. Phys. Oceanogr.* 6(6), 925-930. doi:http://dx.doi.org/10.1175/1520-0485(1976)006<0925, OTIBLA>2.0.CO;2.
- Glejin, J., Sanil Kumar, V., Balakrishnan Nair, T.M., 2013. Monsoon and cyclone induced wave climate over the near shore waters off Puduchery, south western Bay of Bengal, *Ocean Eng.* 72, 277-286. doi:10.1016/j.oceaneng.2013.07.013.
- Goda, Y., Miura, K., Kato, K., 1981. On-board analysis of mean wave direction with discus buoy, *Proceedings of the International Conference on Wave and Wind Directionality—Application to the Design of Structures*, Paris, pp. 339–359.
- Gonzalez-Rodriguez, D., Madsen, O. S., 2007. Seabed shear stress and bedload transport due to asymmetric and skewed waves, *Coast Eng.* 54(12), 914-929. doi:10.1016/j.coastaleng.2007.06.004.
- Grinsted, A., Moore, J. C., Jevrejeva, S., 2004. Application of the cross wavelet transform and wavelet coherence to geophysical time series, *Nonlinear Proc. Geoph.* 11(5/6), 561-566. doi,10.5194/npg-11-561-2004.
- Hashimoto, N., Nagai, T., Asai, T., 1993. Extension of the maximum entropy principle method for directional wave spectrum estimation, *Hydraulic Engineering Division and Marine Hydrodynamics Division*, 18, 232-246.
- Hasselmann, D.E., Dunckel, M., Ewing, J.A., 1980. Directional wave spectra observed during JONSWAP 1973, *J. Phys. Oceanogr.* 10(8), 1264-1280.
- Herbers, T., Elgar, S., Guza, R., 1999. Directional spreading of waves in the nearshore, *J. Geophys. Res.*, 104(C4), 7683-7693. doi: 10.1029/1998JC900092.

Indian Meteorological report (IMD)- RSMC-Tropical Cyclone Report No. 1/2011 Report on cyclonic disturbances over north Indian Ocean during 2010. <http://www.imd.gov.in/section/nhac/dynamic/RSMC-2010.pdf> last assessed on 5/29/2013 16:00hrs.

Kalnay, E., Kanamitsu, M., Kistler, R., Collins, W., Deaven, D., Gandin, L., Iredell, M., Saha, S., White, G., Woollen, J., 1996. The NCEP/NCAR 40-year reanalysis project, B. Am. Meteorol. Soc. 77(3), 437-471.

Kuik, A., Van Vledder, G. P., Holthuijsen, L., 1988. A method for the routine analysis of pitch-and-roll buoy wave data, J. Phys. Oceanogr. 18(7), 1020-1034.

Lee, C., Jung, J.-S., Haller, M. C., 2010. Asymmetry in directional spreading function of random waves due to refraction, J. Waterw. Port. C.-ASCE 136(1), 1-9.

Longuet-Higgins, M. S., 1969. A nonlinear mechanism for the generation of sea waves, Proceedings of the Royal Society of London. A. Mathematical and Physical Sciences, 311(1506), pp. 371-389. doi: 10.1098/rspa.1969.0123.

Longuet-Higgins, M. S., Cartwright, D. E., Smith, N., 1963. Observations of the directional spectrum of sea waves using the motions of a floating buoy. Ocean Wave Spectra, Proceedings of a conference, Easton, Maryland, pp. 111-136.

Mitsuyasu, H., Tasai, F., Suhara, T., Mizuno, S., Ohkusu, M., Honda, T., Rikiishi, K. 1975. Observations of the Directional Spectrum of Ocean Waves Using a Cloverleaf Buoy, J. Phys. Oceanogr. 5(4), 750-760.

Nelson, R., Gonsalves, J., 1990. A field study of wave reflections from an exposed dissipative beach, Coast Eng. 14(5), 457-477. doi: 10.1016/0378-3839(90)90004-G.

Prevosto, M., 1998. Effect of directional spreading and spectral bandwidth on the nonlinearity of the irregular waves, Proceedings of the Eighth International Offshore and Polar Engineering Conference, Montréal, Canada, May24-29, 1998.

Sanil Kumar, V., 2006. Variation of wave directional spread parameters along the Indian coast, Appl. Ocean Res. 28(2), 93-102. doi: 10.1016/j.apor.2006.07.001.

Sanil Kumar, V., Anjali Nair, M., 2015. Inter-annual variations in wave spectral characteristics at a location off the central west coast of India. Annales Geophysicae 33: 159-167, [www.ann-geophys.net/33/159/2015/](http://www.ann-geophys.net/33/159/2015/).

Sanil Kumar, V., Anoop, T.R., 2013. Directionality and spread of shallow water waves along eastern Arabian Sea, Ann. Geophys. 31, 1817-1827. doi:10.5194/angeo-31-1817-2013.

Sanil Kumar, V., Deo M.C., Anand N.M., Chandramohan, P., 1999. Estimation of wave directional spreading in shallow water, Ocean Eng. 26(1), 83-98. doi: 10.1016/S0029-8018(97)10014-2.

Sanil Kumar, V., Deo, M.C., Anand, N.M., Kumar, K.A., 2000. Directional spread parameter at intermediate water depth, Ocean Eng. 27(8), 889-905. doi: 10.1016/S0029-8018(99)00029-3.

Zhou, Y.H., Zheng, D.W., Liao, X.H., 2001. Wavelet analysis of interannual LOD, AAM, and ENSO: 1997-98 El Niño and 1998-99 La Niño signals. J. Geodesy, 75, 164-168.

Table 1. Monthly variation between onshore, offshore, total wave spectral energy and percentage variation of incident wave and reflected waves during 2010

Month	Percentage		Energy (m <sup>2</sup> /Hz)		Total
	Onshore/ Incident wave	Offshore wave	Onshore/ Incident wave	Offshore wave	
January	94.46	5.54	66.69	3.19	69.88
February	93.29	6.71	34.47	1.97	36.44
March	89.30	10.70	20.62	2.32	22.94
April	89.00	11.00	28.75	3.44	32.19
May	88.91	11.09	61.14	7.28	68.42
June	86.37	13.62	49.00	7.34	56.34
July	86.68	13.32	39.59	5.77	45.36
August	85.46	14.54	41.12	6.48	47.60
September	85.54	14.46	34.85	5.44	40.29
October	86.67	13.33	44.70	6.46	51.16
November	91.00	9.00	85.10	6.30	91.40
December	91.98	8.02	94.63	6.00	100.63

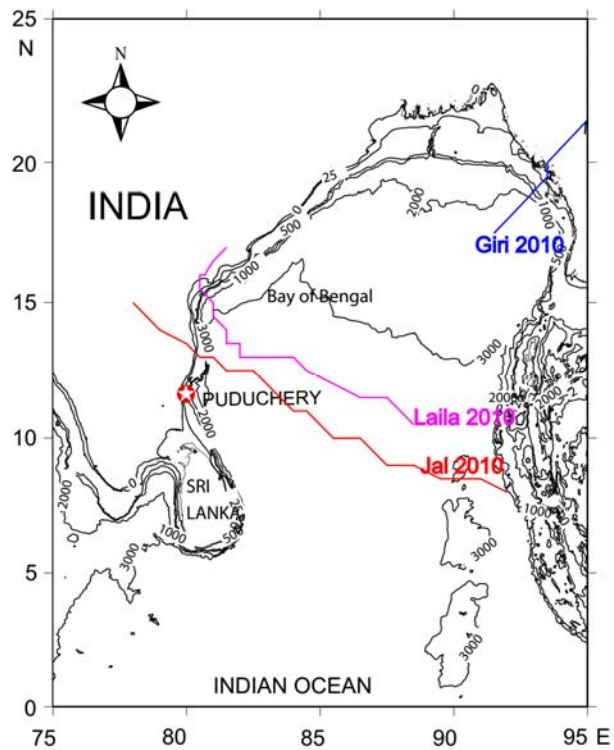


Figure 1. Wave measurement location off Puducherry along the east coast of India in the Bay of Bengal (contours are in metres). The tracks of cyclones (Giri, Laila, and Jal) observed during 2010 are also shown in the figure.

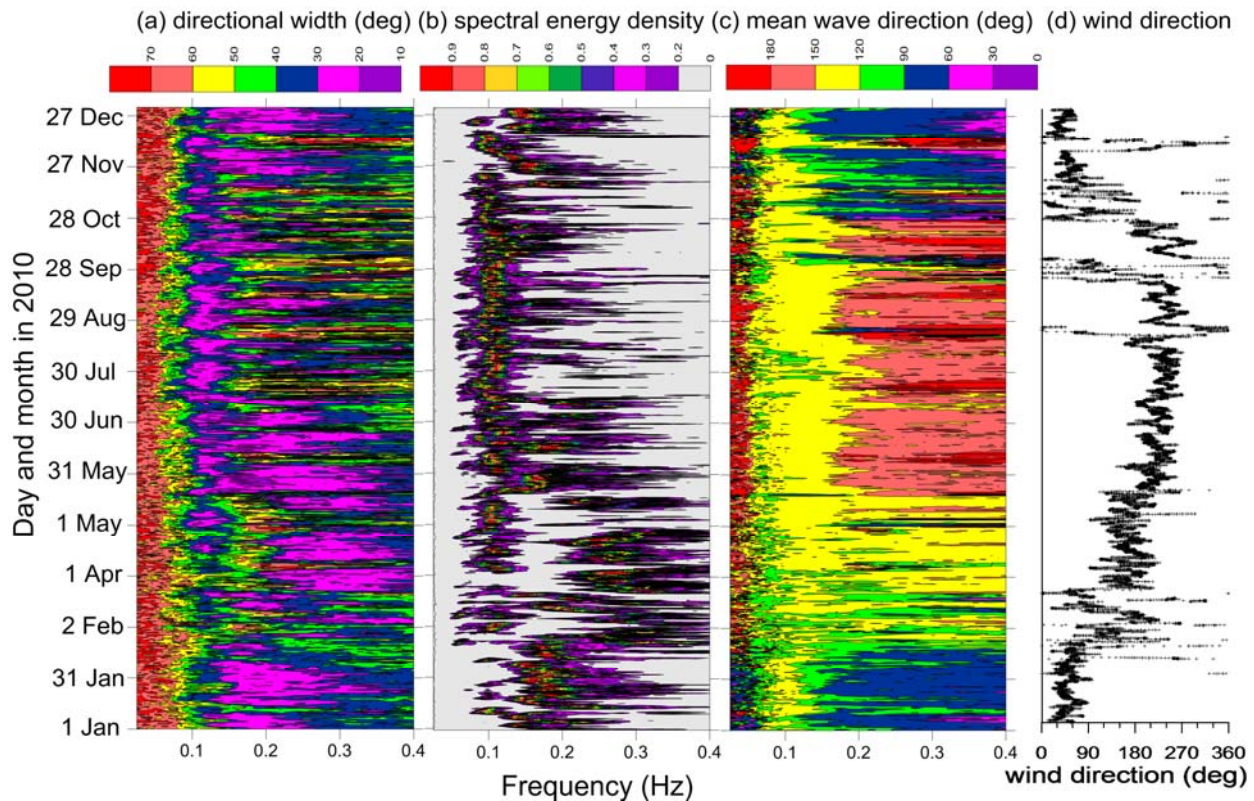


Figure 2. Contour plots of (a) directional spread, (b) normalised spectral energy density and (c) mean wave direction with frequency and time and (d) temporal plot of wind direction during 2010

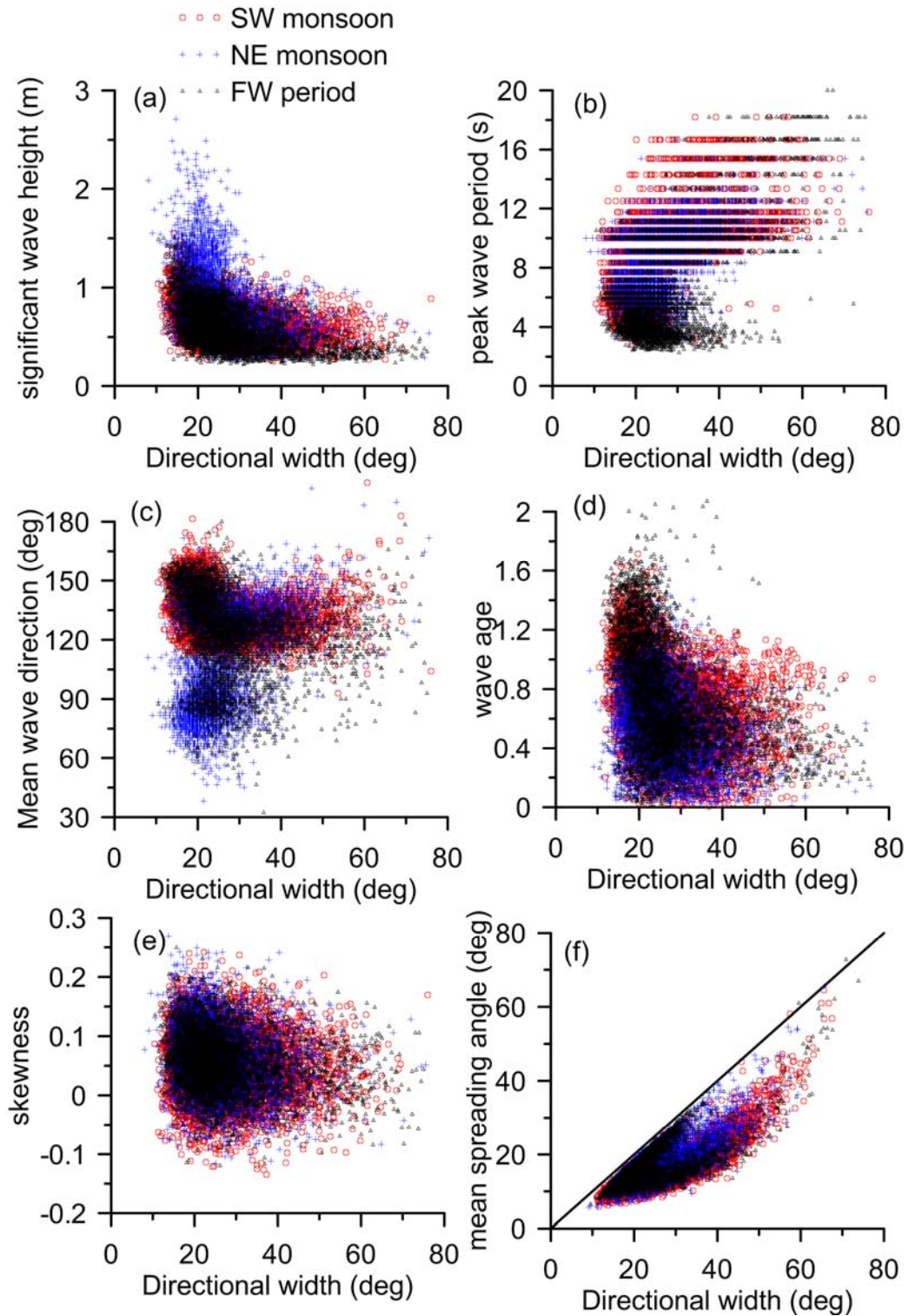


Figure 3. Scatter plots of (a) significant wave height (b) peak wave period (c) mean wave direction (d) wave age (e) skewness and (f) mean spreading angle with directional width

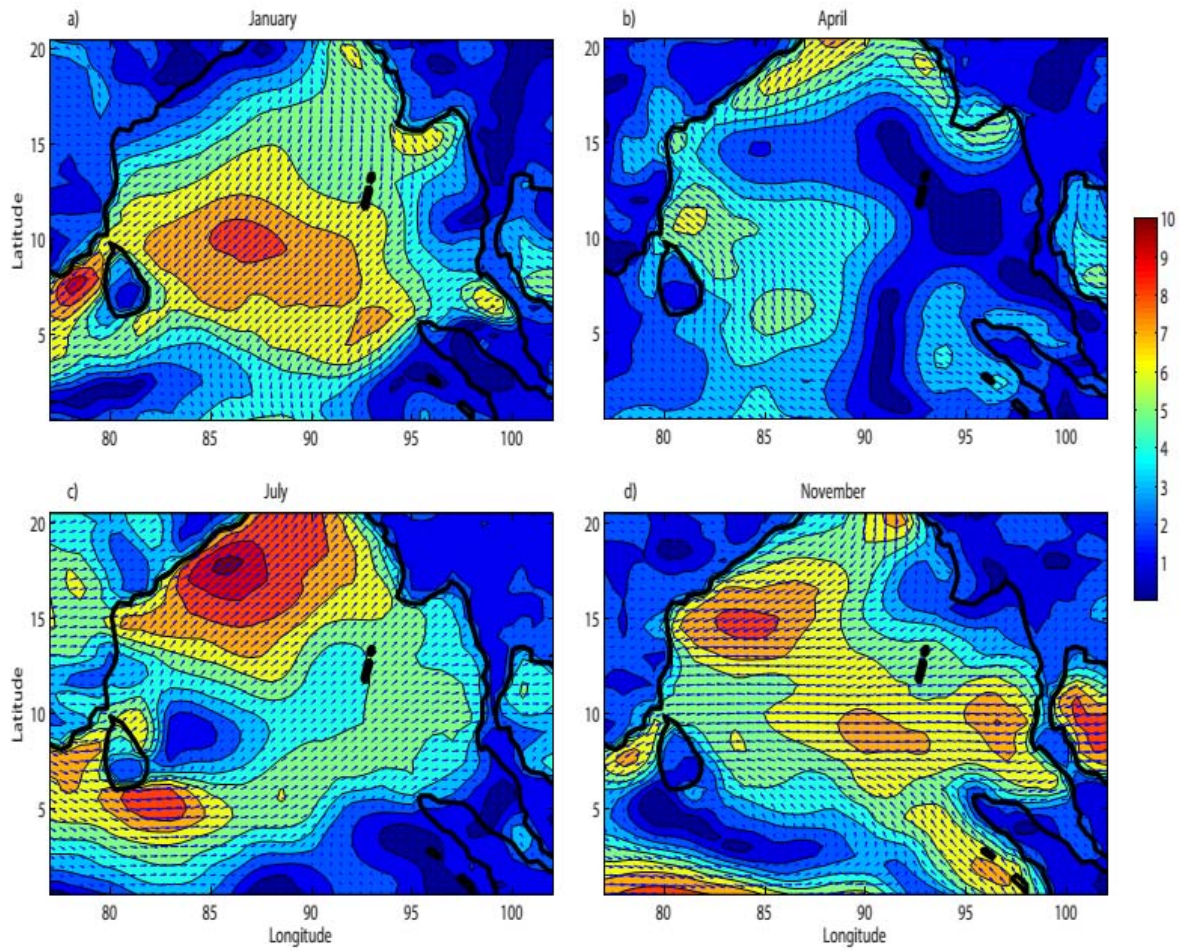


Figure 4. Monthly variation of wind pattern over the Bay of Bengal during different months in 2010. Wind speed is in m/s.

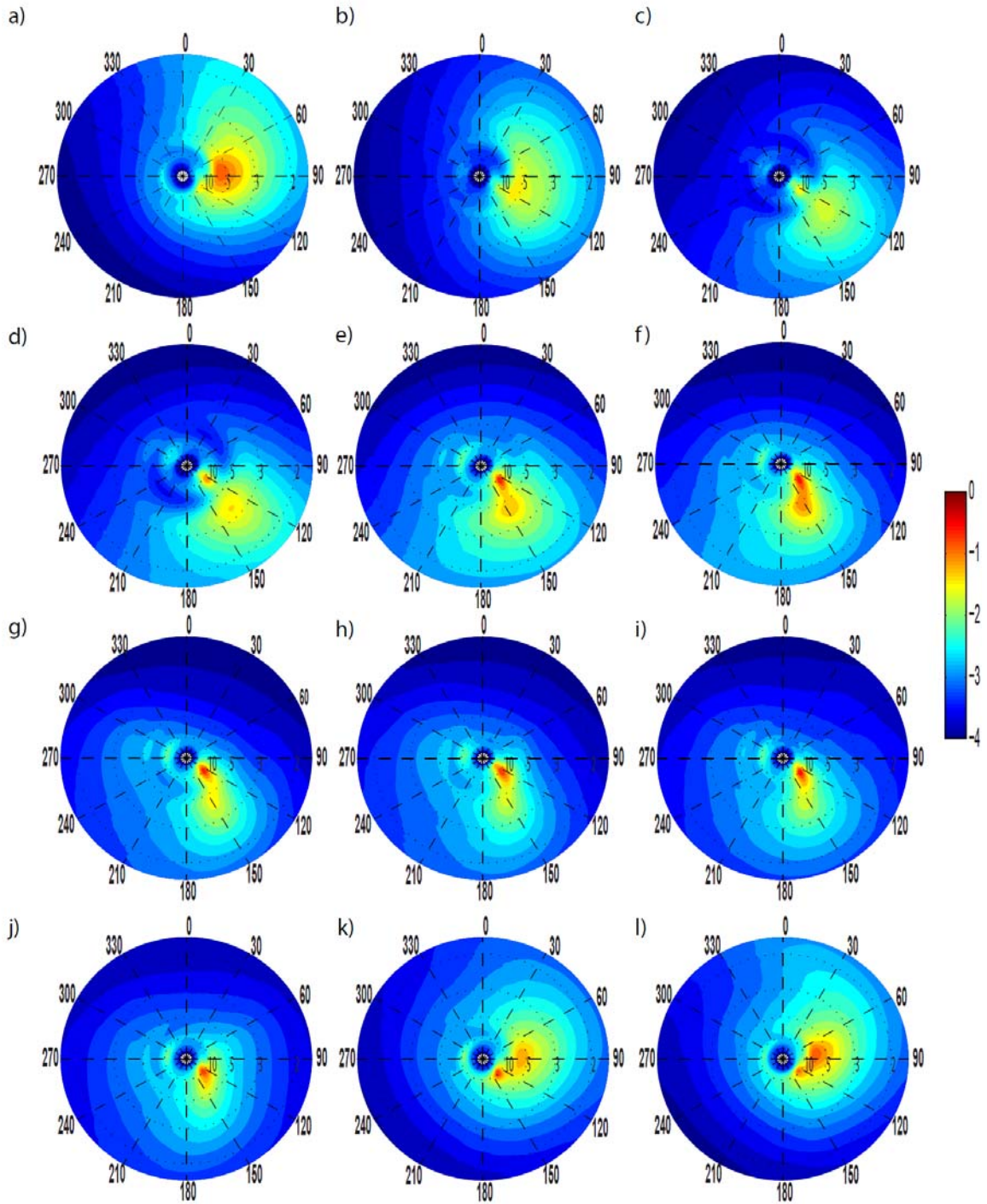


Figure 5. Monthly averaged directional spectrum starting a) January to l) December during 2010 from Puducherry. Contours presented are the spectral energy density in logarithmic scale base to 10

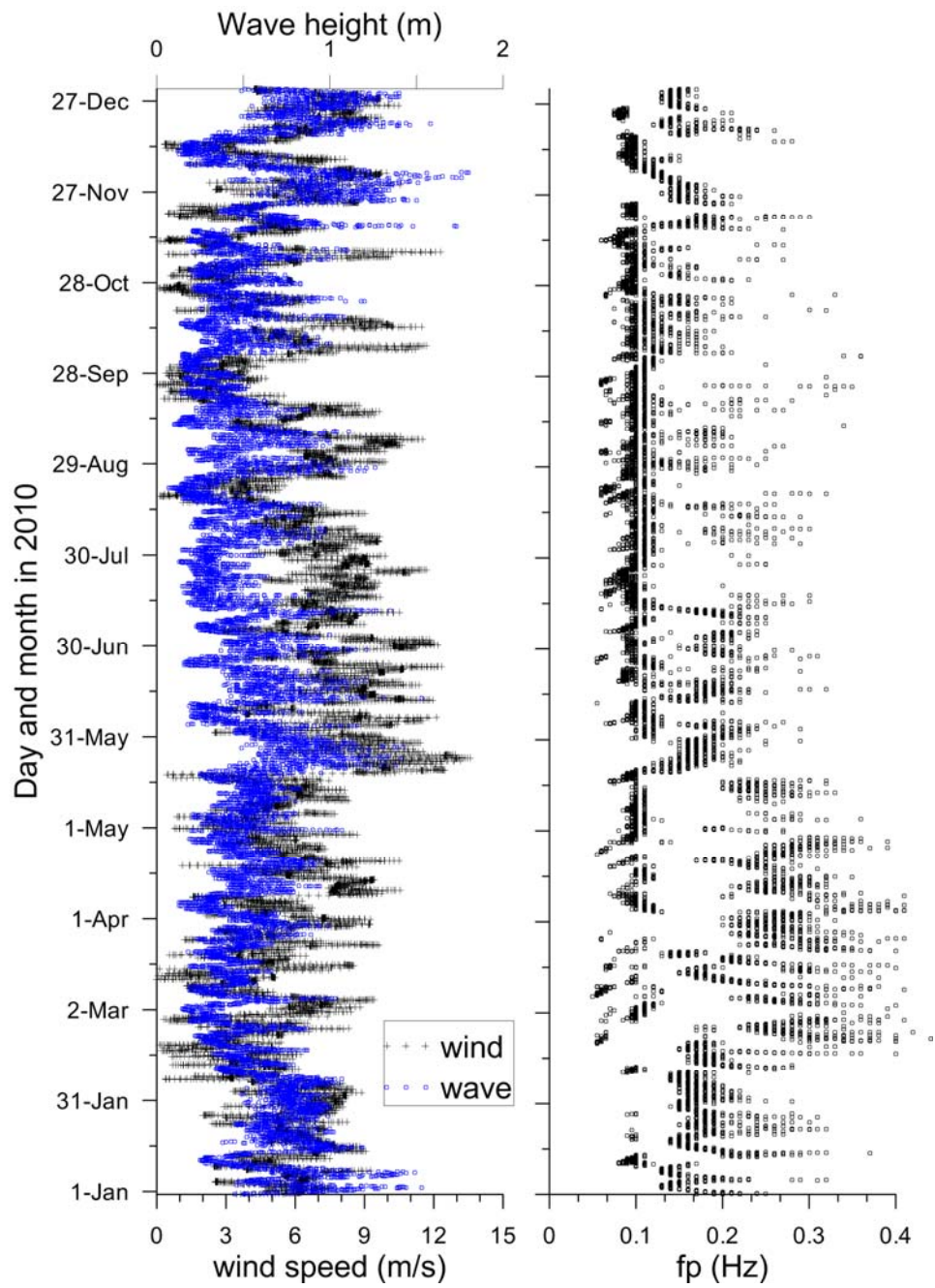


Figure 6. Temporal variation of (a) wind speed and significant wave height of wind-sea and (b) peak frequency



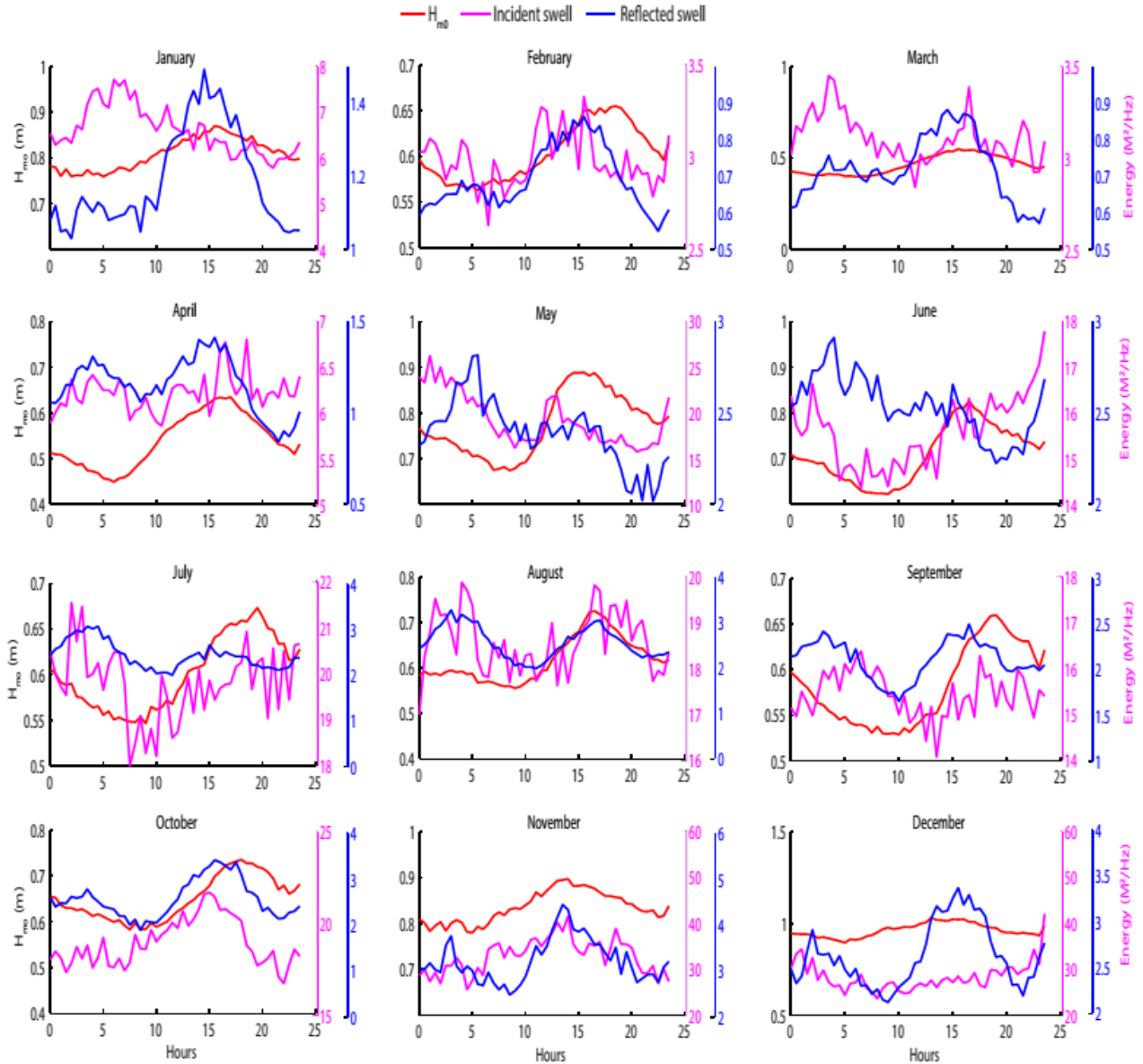


Figure 7. Hourly variation of monthly average significant wave height, incident swell energy and reflected energy during different months in 2010. X-axis represents time in UTC

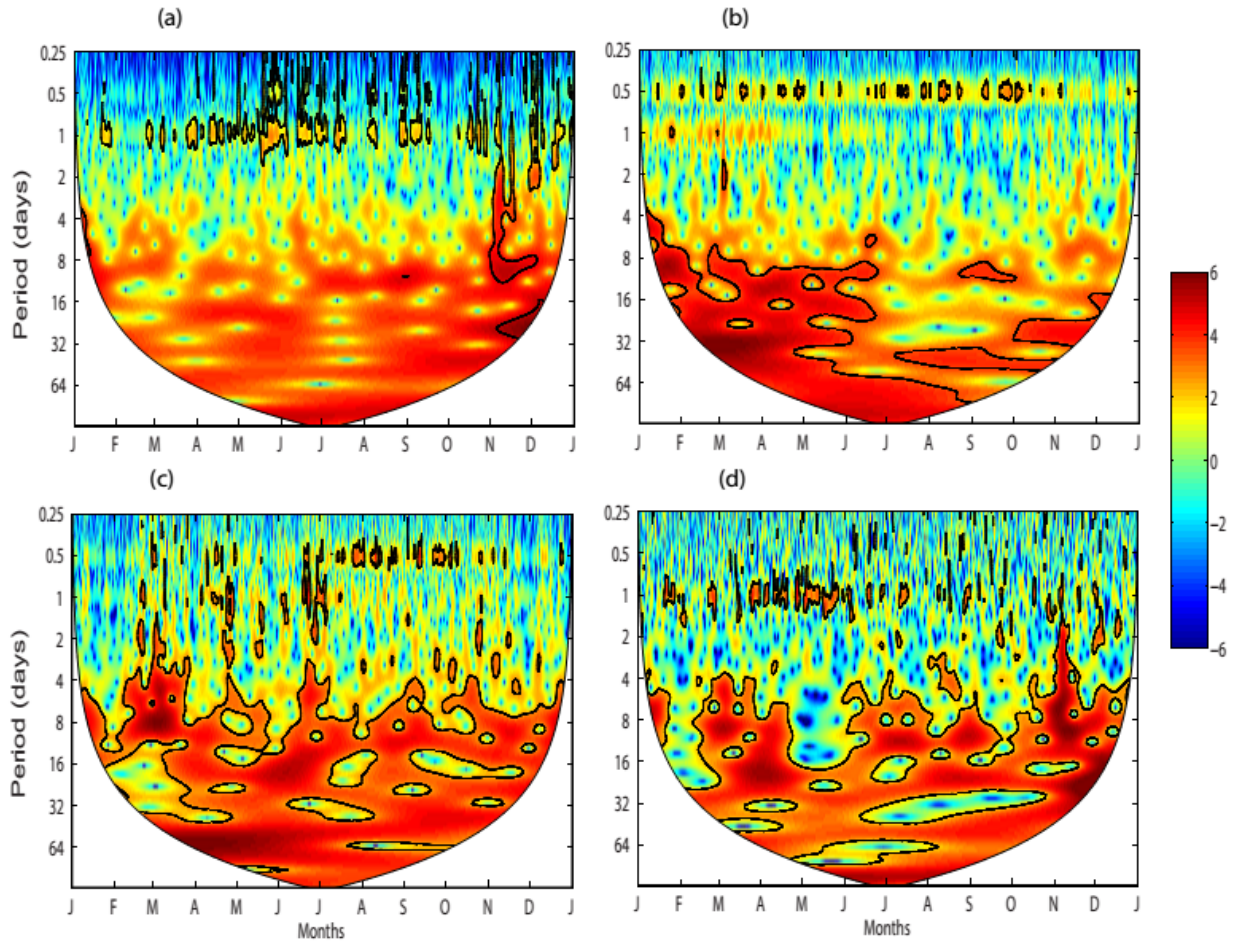


Figure 8. Continuous wavelet power spectrum of wave parameters a) significant wave height b)reflected swell coefficient c) directional width d) skewness

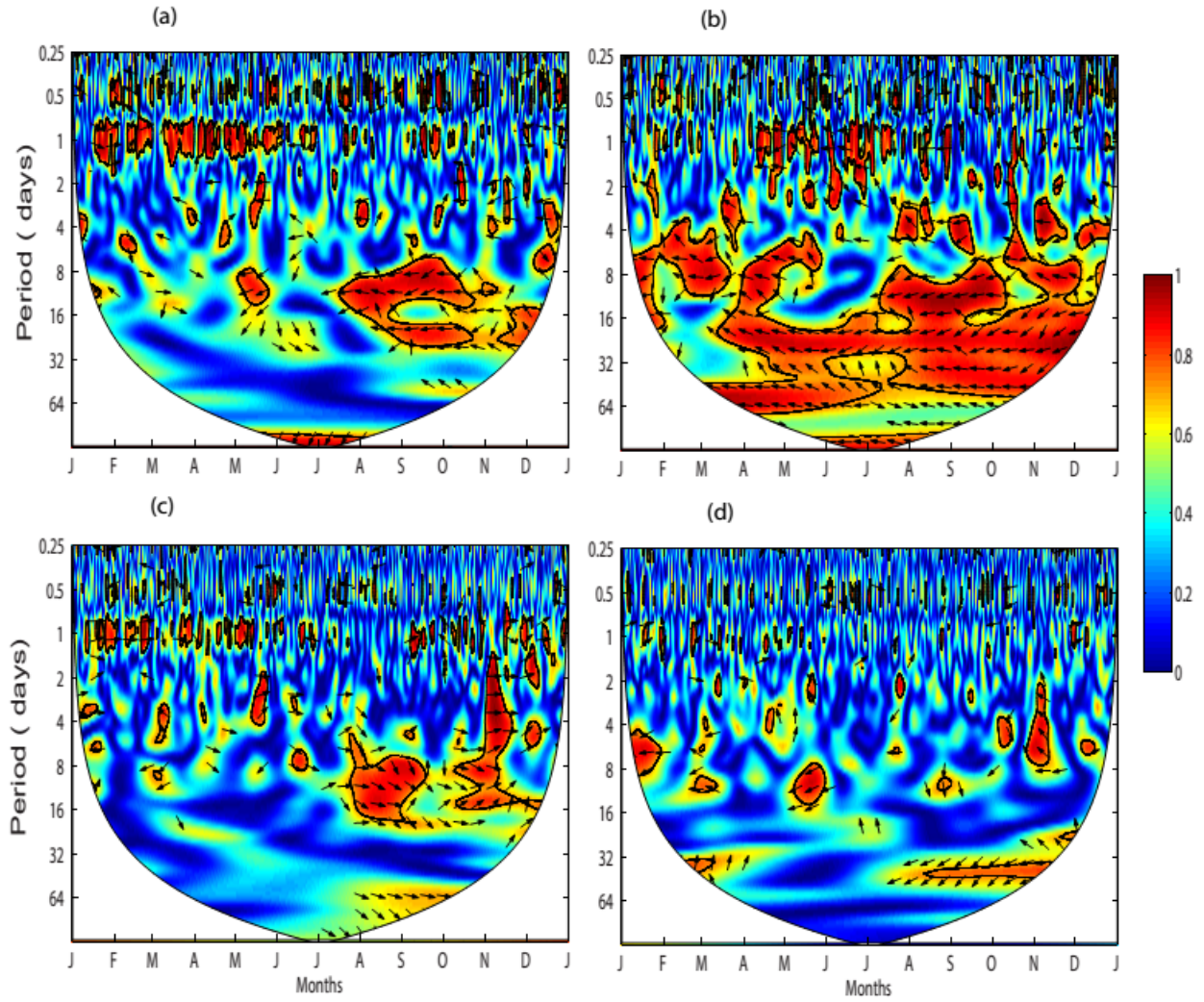


Figure 9. Wavelet coherence spectra between a)  $H_{m0}$  and reflected swell coefficient b)  $H_{m0}$  and directional width c) reflected swell energy and skewness d) reflected swell energy and kurtosis at the near-shore region in the south western Bay of Bengal

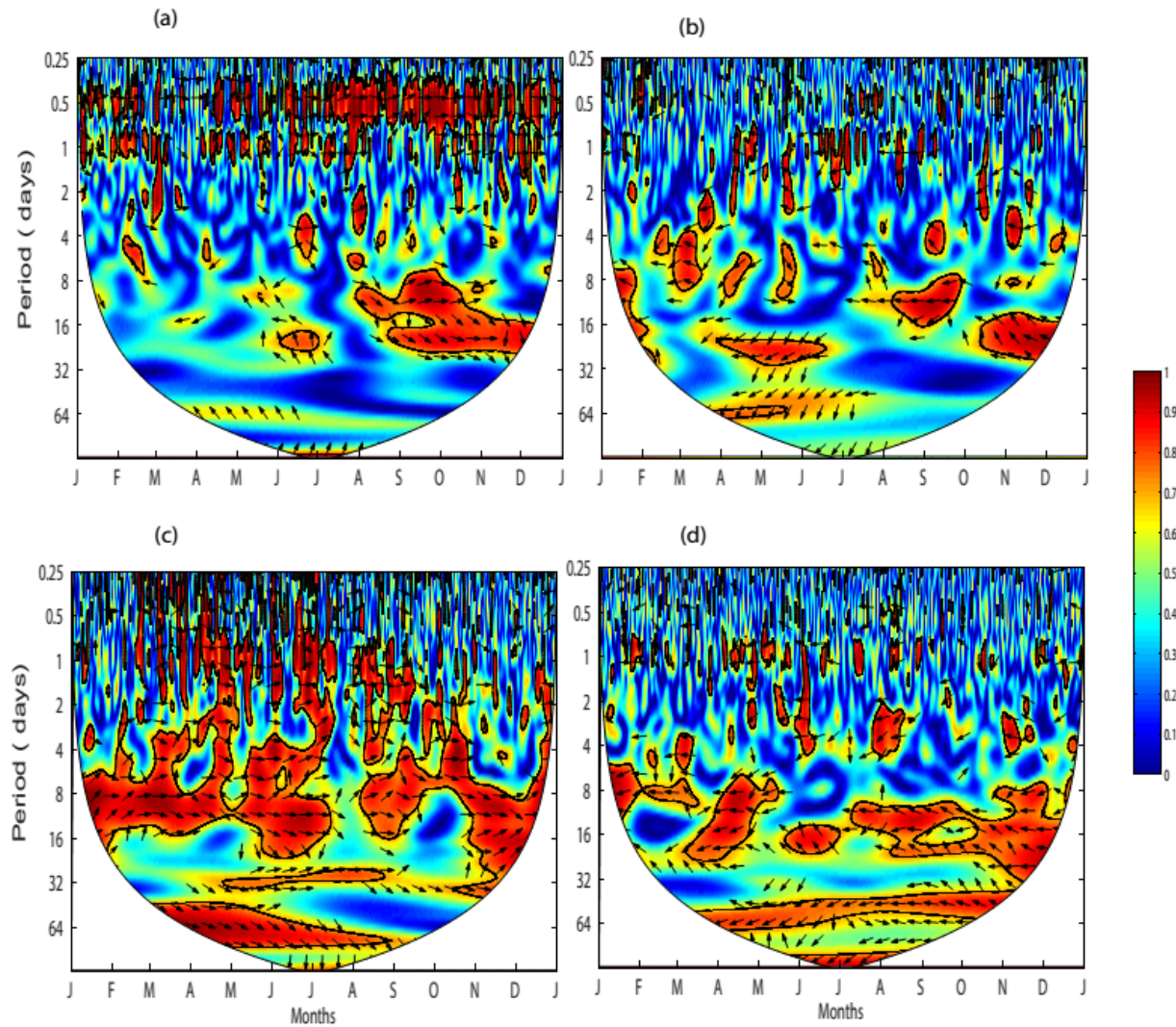


Figure 10. Wavelet coherence between a) directional width and reflected swell coefficient, b) directional width and maximum spectral energy density, c) directional width and peak period, d) directional width and skewness at the near-shore region in the south western Bay of Bengal